CHEMISTRY OF MATERIALS

Article

pubs.acs.org/cm

Experimental Realization of a Unique Class of Compounds: *XY*-Antiferromagnetic Triangular Lattices, $KAg_2Fe[VO_4]_2$ and $RbAg_2Fe[VO_4]_2$, with Ferroelectric Ground States

Ngozi E. Amuneke,[†] Joshua Tapp,[†] Clarina R. de la Cruz,[‡] and Angela Möller*[,†]

[†]Department of Chemistry and Texas Center for Superconductivity, University of Houston, Houston, Texas 77204-5003, United States

[‡]Quantum Condensed Matter Division, Oak Ridge National Laboratories, Oak Ridge, Tennessee 37831, United States

Supporting Information

ABSTRACT: $AAg_2Fe[VO_4]_2$ with A = K or Rb was synthesized by solid state methods and characterized by thermodynamic properties measurements (Néel order at $T_N \approx 3.0$ K). The respective nuclear ($a^{K,Rb} = 5.48$ Å, $c^{K} = 7.212$ Å, $c^{Rb} = 7.357$ Å, $P\bar{3}$, $Z = 1$) and magnetic structures were refined using neutron diffraction in applied magnetic fields. The results indicate enhanced structural stability of the $P\bar{3}$ structure and the realization of a frustrated triangular lattice with antiferromagnetic *XY*-anisotropies. Two magnetic structures were identified: a helical and chiral Y-phase with a propagation vector of (1/3, 1/3, ≈ 0.39) and a commensurate up−up−down phase. These unique compounds offer convenient experimental access for optimizing the features and properties of ferroaxial multiferroic materials.

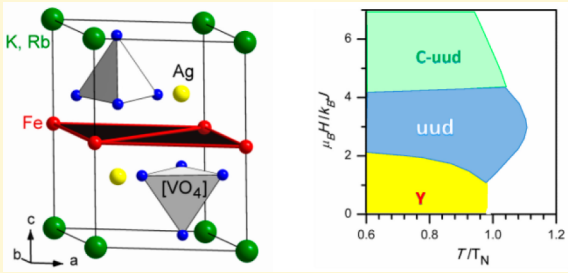

INTRODUCTION

Multiferroic compounds are gaining increasing interest because of their potential use in ultrahigh density data storage.[1,2] In particular, multiferroic materials that exhibit simultaneous magnetic and ferroelectric phase transitions are extremely rare and thus the ultimate goal of current research efforts.[3,4] The geometrically frustrated triangular lattice (TL) belongs to a chiral universality class, for which such a rare phenomenon might occur based on symmetry arguments.[5,6] The features of the TL with *XY*-anisotropies have been extensively studied by theory, and magnetic phase diagrams have been calculated.[7−11] Until now, only a limited number of compounds have been confirmed to exhibit these outstanding properties related to chiral (120°) magnetic ground states, e.g., $ACrO_2$ with A = Cu and Ag,[12,13] $Ba_3NiNb_2O_9$,[14] and $RbFe[MoO_4]_2$.[15,16] Thus, the discovery of new multiferroic materials is needed to understand and address experimentally the dependencies on structural aspects, thermal and quantum fluctuations, magneto-elastic effects, and the coupling of chiral magnetic phases to the polarization.

This work focuses on the geometrically frustrated triangular lattice (TL)[17] with magnetic *XY*-anisotropy. At present, members of the $AFe[TO_4]_2$ type of compounds, where A = K, Rb, or Cs and T = S or Mo, have been identified as the best candidates.[18−22] However, polymorphism has been reported for several cases, e.g., a structural phase transition occurs from $P\bar{3}m1$ to $P\bar{3}$ at 190 K for $RbFe[MoO_4]_2$.[23] Upon cooling, $KFe[MoO_4]_2$ undergoes even a second phase transition into a monoclinic structure, which gives rise to an entirely different magnetic order.[24] In order to retain perfect geometrical frustration, structural distortions must be suppressed. Among these $AFe[TO_4]_2$ type candidates, those without a mirror-plane and preserved 3-fold symmetry, e.g., $P\bar{3}$ space group, should qualify for a transition into a ferroelectric magnetic phase below the Néel temperature, T_N.[5,6] Here, we introduce a series of chemically modified compounds, $AAg_2Fe[VO_4]_2$ with A = K or Rb, crystallizing in the space group $P\bar{3}$, where structural phase transitions are suppressed up to ∼600 K due to the incorporation of additional nonmagnetic ions (Ag^+).

Presumably the most intensively studied compound is $RbFe[MoO_4]_2$, for which the closest realization of a TL antiferromagnet with *XY*-anisotropy has been established.[15,16,20−23] The antiferromagnetic ground state at zero fields ($T_N = 3.8$ K) is remarkable since it is chiral (120° order of magnetic moments in the *ab*-plane), and ferroelectric with a helical order along the *c*-direction, compare to Figure 1 (Y-phase). It should be noted that the emerging multiferroelectricity is a feature of the space group symmetry (here $P\bar{3}$) and not due to the incommensurate order.[5,6] In a recent paper, evidence for the ferroaxial multiferroic properties were given, and the coupling of magnetic chiralities to the ferroelectric polarization were established.[25] The interesting questions arising here are the interplay of chirality (*ab*-plane), the incommensurate propagation along [001], and the electrical

Received: July 14, 2014
Revised: September 21, 2014
Published: September 23, 2014

 © 2014 American Chemical Society dx.doi.org/10.1021/cm5025712 | Chem. Mater. 2014, 26, 5930−5935

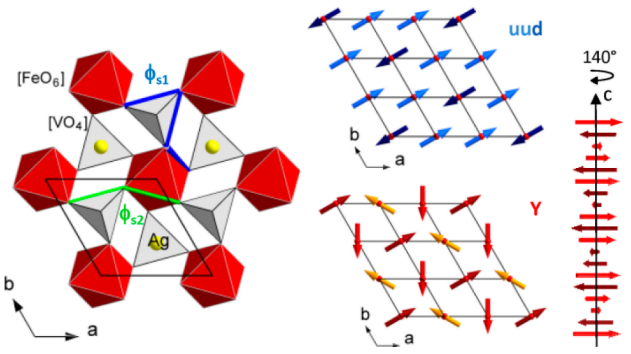

Figure 1. Left: Single Fe-based TL connected via $[VO_4]$ units and supported by Ag-ions in $AAg_2Fe[VO_4]_2$ with A = K or Rb. ϕ_{s1} represents the relative orientation of $[VO_4]$ with respect to the magnetic ions and ϕ_{s2} the deviation from 180°. Middle: Magnetic structures of the uud- (blue) and Y-phases (red). Note the chirality for *Y*. Right: Helical order along [001] for Y.

polarization, from which ferroaxial multiferroicity might originate.

EXPERIMENTAL SECTION

Synthesis of powder samples of $AAg_2Fe[VO_4]_2$ with A = K, Rb, Ag were performed by solid state techniques using stoichiometric amounts of K_2CO_3 (anhydrous, 99%, Alfa Aesar), Rb_2CO_3 (anhydrous, 99.9%, Alfa Aesar) or Ag_2O (Pfaltz & Bauer, Inc.), $AgVO_3$ (synthesized from Ag_2O and V_2O_5 (Alfa Aesar)), and Fe_2O_3 (hydrated, catalyst grade, 30−50 mesh; Sigma-Aldrich Chemie). The reaction temperature was kept below 773 K (3 d). The products were reground and pelletized again for several annealing procedures. The samples were checked for phase purity by X-ray diffraction (X'Pert Pro PANanalytical; Anton Paar, Cu−Kα_1 = 1.5406 Å and Cu−Kα_2 = 1.5444 Å) and evaluated by profile-fitting routines.[26] Differential scanning calorimetry measurements were carried out using a Mettler Toledo Gas Controller DSC System (20 K/min, Al-crucibles, up to 773 K).

Magnetic susceptibility and specific heat data were collected on powder pellets using a physical property measurement system (PPMS, Quantum Design) in magnetic fields of up to 8 T. Magnetic susceptibility were investigated using field cooled (FC) as well as zero-field cooled (ZFC) experiments, and the data was corrected for diamagnetic contributions.

Neutron diffraction data was collected using the HB-2A high-resolution powder diffractometer (ORNL) at a wavelength of λ = 2.406 Å with a Ge(113) monochromator and 12′-31′-6′ collimation, temperature range 1.3 to 20 K in applied fields up to 5 T. Correction of the data included Al as a contributing phase due to shielding and container material. Approximately 9.0 g of $KAg_2Fe[VO_4]_2$ was pressed into 6 mm pellets of 1 g each, stacked, and loaded in a vanadium can; 9.8 g of $RbAg_2Fe[VO_4]_2$ powder were pressed into 4 mm thick 8 mm diameter pellets, stacked and loaded into a 12 mm diameter aluminum can. Data was collected for samples run from 10° to 131° (in 2θ) with steps of 0.1173° for $KAg_2Fe[VO_4]_2$ and 0.065° for $RbAg_2Fe[VO_4]_2$ with scan times of 60 s/step. Field-sweep measurements for $RbAg_2Fe[VO_4]_2$ were collected in steps of 0.1501°. Neutron diffraction data was refined using the program FullProf.[26]

RESULTS

Crystal Structure. The structure of $AAg_2Fe[VO_4]_2$, with A = K or Rb, is shown in Figure 1. Table 1 lists the refined lattice constants. The atomic positions, interatomic distances, and further details of the refinement are provided in the Supporting Information. The average interatomic distances, $d(Fe^{3+}-O)$ = 2.0 Å and $d(V^{5+}-O)$ = 1.70 Å, are typical for $[FeO_6]$ and $[VO_4]$ complex units of D_{3d} and C_{3v} symmetry, respectively.

Table 1. Refined Lattice Parameters in Å and Cell Volumes in Å^3 for $AAg_2Fe[VO_4]_2$ with A = K or Rb ($P\bar{3}$, Z = 1)

T	20 K[a]	1.5 K[a]	293 K[b]
a^K	5.48099(7)	5.4811(1)	5.4896(1)
c^K	7.2119(1)	7.2119(1)	7.2430(1)
V^K	187.629(5)	187.631(5)	189.03(1)
a^{Rb}	5.47563(3)	5.47556(6)	5.4827(1)
c^{Rb}	7.35696(8)	7.35685(9)	7.3826(1)
V^{Rb}	191.028(3)	191.022(3)	192.19(1)

[a]Neutron data. [b]X-ray data.

Within a layer, adjacent magnetic ions (Fe^{3+}, d^5 configuration, S = 5/2) connect exclusively via vanadate ions. Thereby, a geometrically frustrated TL is formed. The crucial dependence of the orientation of the $[VO_4]^{3-}$ units is noteworthy. Neither the relative rotation of the vanadate (ϕ_{S1}) nor a shift along the *c*-axis destroys the space group symmetry. This provides a sensitive tool for tuning the magnetic exchange by chemical and physical pressure.[27,28] Since the vanadate ions are orientated in an up−down arrangement with respect to the planar Fe-based TL, there exist voids opposing each location. These sites are filled by Ag ions in a distorted tetrahedral coordination here but remain unoccupied for $AFe[TO_4]_2$. Thus, structural stability is achieved for the former in the entire temperature region below 600 K (DSC measurements, see Supporting Information). The out-of-plane O^{2-} ions connect exclusively to Ag and the A-site cations (K or Rb, not shown here), which separate the TL-layers.

Comparing the two vanadate structures one finds rather similar *a*-lattice constants for both compounds, which mark the Fe−Fe interatomic distances within the TL. The Fe−Fe interlayer distance is set by the respective *c*-lattice constant, which depends on the size of the A-cation. The *c*/*a* ratio amounts to ∼1.32 and 1.34 for A = K and Rb, respectively. Since the vanadate ion can be considered a rigid complex unit, a slight rotation ($\Delta\phi_{s2}$ = 4.5°) accompanied by a small shift along [001] results. This reveals the structural difference between the K and Rb compounds.

Thermodynamic Properties. This work reports the properties of $KAg_2Fe[VO_4]_2$ and $RbAg_2Fe[VO_4]_2$, respectively, showing the excellent realization of the antiferromagnetic TL with *XY*-anisotropy. The magnetic phase diagrams (Figure 2) were constructed based on thermodynamic data; see also Supporting Information. The emerging ordered magnetic

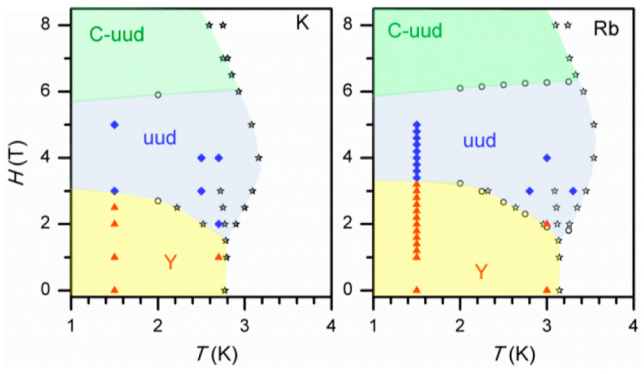

Figure 2. (a) Temperature versus magnetic field phase diagrams for $AAg_2Fe[VO_4]_2$ with A = K or Rb. Data points: $M(H)$ (circles), $C_p(T)$ (stars), and neutron data (triangles and diamonds).

dx.doi.org/10.1021/cm5025712 | *Chem. Mater.* 2014, 26, 5930−5935

phases, Y and uud (up−up−down) under applied fields up to 5 T were studied and confirmed by neutron diffraction experiments, see below.

The susceptibility data, $\chi(T)$, are found to be independent of zero-field and field cooling modes. The magnetic moment, μ^{eff}, per Fe^{3+} at 300 K is reduced by ∼10% to 5.4 μ_B, comparable with other S = 5/2 TL compounds. At high temperatures, $1/\chi(T)$ can be fitted to a Curie−Weiss law. The Weiss constant, $\Theta_{\text{C-W}}$, is found at ∼−20 K. A maximum in $\chi(T)$ at $T_N \approx 3$ K indicates the antiferromagnetic long-range ordered state (Figure 3a). For geometrically frustrated systems like TL, one

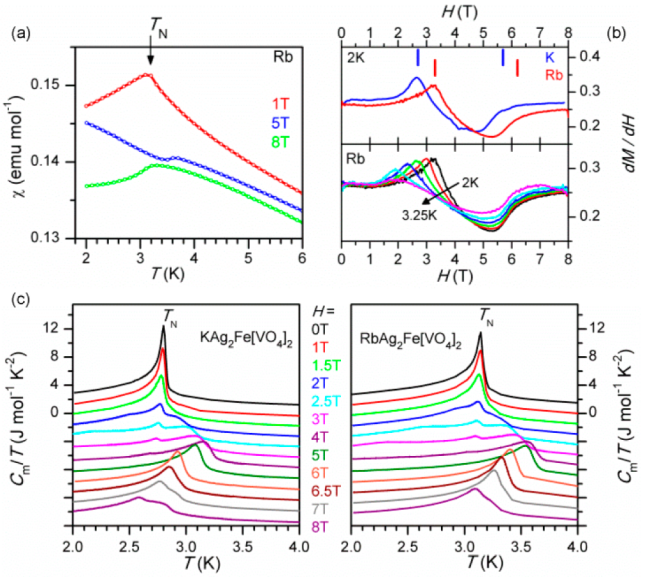

Figure 3. (a) Susceptibility, $\chi(T)$, at various fields for $RbAg_2Fe[VO_4]_2$. (b) Derivatives of the magnetization, dM/dH, for $AAg_2Fe[VO_4]_2$ with A = K or Rb. Markers indicate the range of the magnetization plateau at ∼1/3M_s. (c) Field dependence of the magnetic specific heat, C_m/T (note the shift of −1.5 J mol^{-1} K^{-2} per graph for increasing fields).

expects large ratios of $|\Theta_{\text{C-W}}|/T_N$, here ∼7, similar to other members of the $AFe[TO_4]_2$ family.[19,29,30] Below T_N the temperature dependence of $\chi(T)$ changes drastically at higher fields, corresponding to the different magnetic structures depicted in Figure 1, the canted-uud (C-uud) one at the highest field measured.

The field-dependent magnetization, $M(H)$, shows a plateau in the magnetically ordered regime as indicated by the respective derivatives dM/dH (Figure 3b). The onset at lower fields of ∼2−3 T corresponds to the phase transformation from the ferroelectric spiral Y-phase into the commensurate uud-phase. As established by theory,[7,8] this occurs around the emerging characteristic plateau close to 1/3 of the magnetization saturation, M_s. The uud-phase is stable up to the upper end of the plateau, denoted by $1/3H_s \approx 6.5$ T, with H_s being the saturation field. Thus, one should expect the fully recovered paramagnetic state for these compounds at high magnetic fields of $H_s \approx 20$ T. It is interesting to note that the onset of the plateau is extremely temperature sensitive, highlighting the importance of thermal fluctuations (see neutron diffraction data below).

The magnetic specific heat, $C_m(T)$, was obtained from the measured total specific heat, $C_p(T)$, after subtracting the nonmagnetic lattice contribution ($BaAg_2Mg[VO_4]_2$; for reference, see refs 27 and 28, and the Supporting Information). In Figure 3c, we present the specific heat data evaluation. $C_m(T)$ shows in zero-field a sharp λ-anomaly at T_N = 2.8 and 3.2 K, respectively, indicating a direct phase transition from the paraelectric and paramagnetic high-temperature to the magnetically ordered Y-phase. Within the field range of the above-mentioned magnetization plateau, the uud-phase is expected. With applied fields, the λ-anomaly decreases in magnitude and vanishes; while a broader feature above $H \approx 2$ T develops toward higher temperatures. Simultaneously, a weak second broad feature emerges at lower temperatures, following the $T-H$ dependence of the onset of the 1/3 magnetization plateau (see also Figure 3b). Note that no sharp anomaly is seen around the upper borderline of the plateau, where the uud-phase transitions into the expected canted commensurate uud-phase. At the highest fields measured here (above ∼6.5 T), a shoulder appears at higher temperatures, which marks the transformation into the regime where an incommensurate, canted-uud-phase is expected. The overall spin entropy, S_m, released above 2 K amounts to ∼80% of the total expected value for a S = 5/2 system. At all measured fields, this value is reached, but the inflection point shifts to higher temperatures as expected due to the ferro-type of alignment of two moments in the uud-phases (see Figure 1).

Magnetic Structures. Neutron diffraction data provide evidence for the chiral and helimagnetic ground state (Y) below the respective order temperatures, T_N, in zero field. This is considered a fingerprint of the realization of a TL with XY-anisotropy. The phase transitions upon applied field were investigated, and the respective magnetic structures determined by Rietveld refinement[26] (see Figure 4 and the Supporting

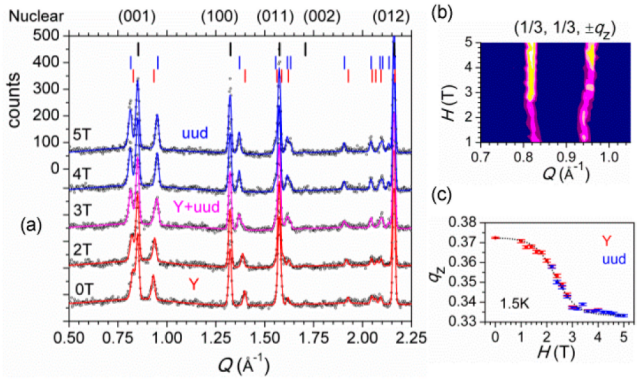

Figure 4. (a) Neutron diffraction data at 1.5 K in fields up to 5 T for $RbAg_2Fe[VO_4]_2$. Markers indicate Bragg positions for the respective phases. (b) Intensity of the magnetic reflections around the nuclear (001) for field-sweep measurements after subtraction of the nuclear contribution. (c) Refinement of q_z in fields up to 5 T. The line serves as a guide to the eye.

Information for details). In good agreement with $\chi(T)$, $M(H)$, and $C_m(T)$, we find evidence for the assigned Y- and uud-phases, respectively. Below, we discuss our findings in relation to the molybdates and emphasize the characteristic features of a TL with an in-plane arrangement of the magnetic moments (XY-anisotropy) proposed by theory.[7−11]

From the refinement and evaluation of the magnetic structures, we established the existence of the 120° structure (Y-phase) in zero field below T_N (see Figures 1 and 4). This phase orders incommensurate ($q_z \neq 1/3$) with a propagation vector k_z = (1/3, 1/3, q_z) along the c-axis. The magnetic rotation angle ϕ_m for the propagation along the c-axis can be

dx.doi.org/10.1021/cm5025712 | Chem. Mater. 2014, 26, 5930−5935

estimated by the relation $2\pi q_z$ and observed at 1.5 K in zero field for $KAg_2Fe[VO_4]_2$, q_z = 0.4035(6), ϕ_m = 145°; and $RbAg_2Fe[VO_4]_2$, q_z = 0.3724(3), ϕ_m = 134°, respectively. As it can be inferred by a comparison with the molybdates ($RbFe[MoO_4]_2$, q_z = 0.458, ϕ_m = 164°; and $CsFe[MoO_4]_2$, q_z = 0.5, ϕ_m = 180°),[15,31] this parameter neither relates to the interplane separation, which is a function of the A-cation size, nor to the respective T_Ns in a straightforward relationship. We also note that no further insights can be gained from a structural perspective. Namely, the dihedral angles $\phi_{s1} \approx 121°$ and rotation angles ϕ_{s2} = 150−158° (Figure 1) are all similar and unrelated to the large differences in ϕ_m. The ordered magnetic moments per Fe^{3+} at zero-field are 3.0 μ_B $KAg_2Fe[VO_4]_2$, 3.3 μ_B $RbAg_2Fe[VO_4]_2$, 3.9 μ_B $RbFe[MoO_4]_2$,[15] and 4.0 μ_B $CsFe[MoO_4]_2$[31] and follow the trend of their respective Néel temperatures.

Note the significantly larger ordered magnetic moments found for the molybdates. This indicates an even larger disordered fraction of the magnetic moment per Fe^{3+} below T_N for the vanadates and calls for further theoretical work to explore the cause. One might speculate that chemical differences of the magnetic superexchange pathway via d(Fe)−p(O)−d(V vs Mo)−p(O)−d(Fe) or the impact of incorporated nonmagnetic Ag ions into the structure are of relevance here. Overall, the ordered magnetic moments for both series of compounds representing TL antiferromagnets with *XY*-anisotropy are found to be significantly reduced when compared with the paramagnetic moment of a $S = 5/2$ system.

To explore the phase transition from the incommensurate Y-phase into the commensurate uud-phase at low temperatures, we performed a field-sweep series for $RbAg_2Fe[VO_4]_2$ at 1.5 K. In Figure 4b,c, we show the field dependence of the order parameter q_z. It is noteworthy that q_z shifts toward 1/3 from 2.5−3.2 T at 1.5 K for the Y-phase, consistent with the onset field of the $1/3M_s$ plateau in the magnetization. Here the in-plane magnetic moments start aligning in an uud fashion, thereby removing the chirality and establishing the commensurate order along the [001]. This transition has been noted by theory to occur for temperatures associated with fields corresponding to the magnetic exchange constant *J*, namely, $H = 2{\cdot}J$ and $3{\cdot}J$, respectively.[7,8] However, a two-magnetic phase refinement of the experiment marks the gradual change from the Y- to the uud-phase and is shown for the 3 T measurement with phase contribution ratio of ∼1:3 (see also intensity and positional changes of magnetic diffraction peaks in Figure 4). Above ∼3.4 T the uud-phase is stabilized with a magnetic moment per Fe^{3+} of 3.1 $\mu_B{}^K$ and 3.4 $\mu_B{}^{Rb}$ (two Fe^{3+} in an antiferromagnetic collinear alignment with one Fe^{3+}).

Thermal fluctuations may be accounted for in the regime between the decreasing λ-anomaly and the higher temperature shoulder at fields where the paramagnetic to uud-phase transition occurs. Neutron data refinements at higher temperatures (2.8−3.3 K) indicate that the calculated ordered effective magnetic moments are smaller (∼2.7 to 2.9 μ_B) in this region. One might speculate that the thermal fluctuations create an effectively reduced averaged moment per Fe^{3+} with its contributors oscillating about their ordered orientation, which is finally established upon reaching the temperature of the vanishing anomaly or by increasing fields.

■ DISCUSSION

On the basis of the crystal structure, it is intriguing to note that the *a*-lattice constants are similar for both title compounds (a^K = 5.481 Å and a^{Rb} = 5.476 Å). Thus, one might expect similar exchange constants within the TL. Applying the theoretical relationships: $M = J{\cdot}H/9$, $T_N = 0.5{\cdot}J{\cdot}S^2$, and $H_s = 9{\cdot}J$, we calculate J = 0.98(5) K for $RbAg_2Fe[VO_4]_2$ and J = 0.85(5) K for $KAg_2Fe[VO_4]_2$. However, on the basis of the difference in the ionic radii of K^+ and Rb^+, the layer separation (c^K = 7.212 Å and c^{Rb} = 7.357 Å) increases and also the transition temperature into the magnetically long-range ordered state (K, T_N = 2.8 K; Rb, T_N = 3.2 K); see Figure 3. This is an unexpected and highly surprising result. In comparison, the *c*-lattice constants are even longer for $RbFe[MoO_4]_2$ (c = 7.438 Å and T_N = 3.8 K)[23] and $CsFe[MoO_4]_2$ (c = 7.979 Å and T_N = 4.5 K),[31] respectively. As a result, one can rule out that the transition is of "simple" electrostatic origin based on stacking distances. The observations rather confirm the importance of the proposed Dzyaloshinskii−Moriya contribution for the development of a sizable moment in [001].[15] From single-ion ligand field calculations, it can be inferred directly that the *XY*-anisotropy develops a splitting between χ^X and χ^Y at different temperatures depending on the distortion angle, ∠(O−Fe−O), of the $[FeO_6]$ complex in D_{3d} symmetry, e.g., $KAg_2Fe[VO_4]_2$, 88.7° with $\Delta\chi$ below ∼10 K, and $RbAg_2Fe[VO_4]_2$, 89.5° with $\Delta\chi$ below ∼5 K. In principle, the same trend, higher T_N occurring for reduced distortions, is observed also for the Rb- and Cs-molybdates. Hence, significantly different anisotropy parameters, *D* values, should be taken into account and call for further electron spin resonance investigations.

With respect to the magnetic interaction within the TL, the effectiveness of orbital overlap between the Fe-complex and the "linker", $[VO_4]^{3-}$ or $[MoO_4]^{2-}$, might also be important. Qualitative arguments based on the smaller extension of d-orbitals in space for 3d- compared with 4d-transition metal ions (V^{5+} vs Mo^{6+}) directly lead to presumably smaller intraplanar magnetic exchange couplings, *J*. For the molybdates, *J* is reported to be approximately 1.2 K,[20−22] despite larger *a*-lattice constants (a^{Rb} = 5.596 Å; a^{Cs} = 5.565 Å)[23,31] than those for the vanadates. Another aspect we wish to emphasize here is that the charge of the "linker", $[VO_4]^{3-}$ vs $[MoO_4]^{2-}$, should also be considered as a crucial tuning parameter for the evaluation of this class of TL.

The last point we wish to communicate is related to symmetry aspects and how they can be manipulated by chemical substitutions; here, size effect on the A-site (ionic radii, $r(K^+, Rb^+) \approx 1.50$ Å vs $r(Ag^+) \approx 1.00$ Å). The structure of $Ag_3Fe[VO_4]_2$ has been reported.[32] We have synthesized the compound, confirmed the structure by single-crystal diffraction, and studied the thermodynamic properties (see Supporting Information). The compound crystallizes in the monoclinic space group *C*2/*c*, causing the vanadates to tilt out-of plane and thereby removing the 3-fold symmetry required to retain a perfect TL. This distortion is sufficient to suppress the chiral magnetic ground state, and the mirror plane prohibits the emergence of ferroelectricity. Also, $\Theta_{C.-W.} \approx -30$ K is much larger, while T_N = 4.2 K is comparable to the above-discussed cases. This indicates that the average of the three in-plane *J*-couplings arising from the distortion should be similar to the former cases ($J^{Ag} \approx 1.2$ K). However, in comparison, subtle differences are evident and clearly marked by (i) a less sharp maximum in $\chi(T)$ related to T_N, (ii) the rapid development into a $C_m(T) \approx T^3$ dependence below T_N, and (iii) a broadening of the λ-anomaly at high fields, indicating a magnetic phase transition at $H \approx 6$ T (Figure 5 and Table 2).

dx.doi.org/10.1021/cm5025712 | *Chem. Mater.* 2014, 26, 5930−5935

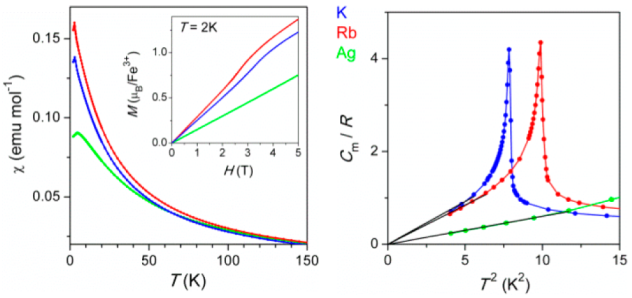

Figure 5. Comparison for $AAg_2Fe[VO_4]_2$ with A = K, Rb, Ag. Left: Susceptibility and magnetization data (inset). Right: Low-temperature fit (black lines represent b_mT) of the magnetic part of the specific heat at zero-field.

Table 2. Comparison of Distances in Å (293 K, X-ray Data), Néel Temperatures and Antiferromagnetic Coupling Constants in K, and b_m Values in K^{-3} for $AAg_2Fe[VO_4]_2$ with A = K, Rb, or Ag

A	K	Rb	Ag
$d(Fe-Fe)^{intra}$	5.49	5.48	5.39[a]
$d(Fe-Fe)^{inter}$	7.24	7.38	7.16[a]
T_N	2.8	3.2	4.2
J	0.85	0.98	1.2
J'	0.033	0.020	0.055
J'/J	0.04	0.02	0.05
b_m	0.18	0.17	0.06

[a]Averaged distances due to lower symmetry.

The magnetic interlayer exchange constants, J', can be estimated from fitting $C_m(T)/R = b_mT^3$ below T_N,[33] where the constant, b_m, relates to J and J' by

$$b_m = \frac{4\pi^2}{15S^3J\sqrt{3J'}}\left[\frac{2}{(9J/2 + 4J')^{3/2}} + \frac{1}{(9J + 4J')^{3/2}}\right]$$

Both title compounds (A = K, Rb) exhibit rather similar b_m factors, which clearly set them aside from the distorted case (A = Ag). We obtained J' values, which reflect the degree of distortion per $[FeO_6]$ unit and the dependence on the layer separation along [001] due to A-cation size effects. It should be noted that, for $Ag_3Fe[VO_4]_2$, adjacent layers alternate with respect to their orientation.

Thus, $Ag_3Fe[VO_4]_2$ might be a good candidate to probe the interplay between the structural distortion and the release of spin frustration under pressure (see also related theoretical work reporting different magnetic phases under applied fields).[34] In a recent paper, polar phases with incommensurate magnetic structures (high-pressure phases) have been established for $CuFeO_2$, a more complicated case involving also several structural phase transitions.[35,36]

CONCLUSIONS

In conclusion, we found that chemical modification of the layer (occupancy of voids with Ag ions) leads to the rare stabilization of an antiferromagnetic TL with *XY*-anisotropy for $KAg_2Fe[VO_4]_2$ and $RbAg_2Fe[VO_4]_2$. We gave detailed features based on thermodynamic and neutron diffraction data and compared these with one of the closest realizations of this unique class of TL materials with *XY*-anisotropies (i.e., the molybdates). These advances will allow an evaluation of the interplay between charge, size, and $[FeO_6]$ distortions with impact on the proposed importance of Dzyaloshinskii–Moriya interactions. Furthermore, we provide insights into chemically induced distortions ($Ag_3Fe[VO_4]_2$) resulting in a remarkable deviation of the properties from the class of perfect geometrically frustrated cases. These results call for further measurements of the electrical polarization including applied pressure experiments and should entice theoretical studies to gain insights into the still unpredictable helicity-related sign of the polarization.

ASSOCIATED CONTENT

Supporting Information

Experimental details of the neutron data structure refinement, interatomic distances, and thermodynamic properties (including data for $Ag_3Fe[VO_4]_2$). This material is available free of charge via the Internet at http://pubs.acs.org.

AUTHOR INFORMATION

Corresponding Author

*E-mail: amoeller@uh.edu.

Author Contributions

The manuscript was written through contributions of all authors. All authors have given approval to the final version of the manuscript.

Notes

The authors declare no competing financial interest.

ACKNOWLEDGMENTS

This work was supported by the National Science Foundation (Grant DMR-1149899) and by the State of Texas through the Texas Center for Superconductivity at the University of Houston. The research at ORNL's High Flux Isotope Reactor was sponsored by the Scientific User Facilities Division, Office of Basic Energy Sciences, U.S. Department of Energy. The authors thank M. Bratsch for help with the DSC measurements.

ABBREVIATIONS

TL, triangular lattice; T_N, Néel temperature; M_s, saturation magnetization; H_s, saturation field; J, magnetic exchange constant (here, antiferromagnetic); R, molar gas constant

REFERENCES

(1) Cheong, S.-W.; Mostovoy, M. *Nature* **2007**, *6*, 13–20.
(2) Tokura, Y.; Seki, S. *Adv. Mater.* **2010**, *22*, 1554–1565.
(3) Johnson, R. D.; Radaelli, P. G. *Annu. Rev. Mater. Res.* **2014**, *44*, 269–98.
(4) Tokura, Y.; Seki, S.; Nagaosa, N. *Rep. Prog. Phys.* **2014**, *77*, 076501.
(5) Ribeiro, J. L.; Perez-Mato, J. M. *J. Phys.: Condens. Matter* **2011**, *23*, 446003.
(6) Perez-Mato, J. M.; Ribeiro, J. L.; Petricek, V.; Aroyo, M. I. *J. Phys.: Condens. Matter* **2012**, *24*, 163201.
(7) Kawamura, H. *J. Phys. Soc. Jpn.* **1985**, *54*, 4530–4538.
(8) Kawamura, H. *Can. J. Phys.* **2001**, *79*, 1447–1458.
(9) Plumer, M. L.; Mailhot, A. *Phys. Rev. B* **1994**, *50*, 16113.
(10) Luca Capriotti, L.; Cuccoli, A.; Tognetti, V.; Verrucchi, P.; Vaia, R. *Phys. Rev. B* **1999**, *60*, 7299.
(11) Seabra, L.; Momoi, T.; Sindzingre, P.; Shannon, N. *Phys. Rev. B* **2011**, *84*, 214418.
(12) Seki, S.; Onose, Y.; Tokura, Y. *Phys. Rev. Lett.* **2008**, *101*, 067204.
(13) Kimura, K.; Nakamura, H.; Ohgushi, K.; Kimura, T. *Phys. Rev. B* **2008**, *78*, 140401(R).
(14) Hwang, J.; Choi, E. S.; Ye, F.; Dela Cruz, C. R.; Xin, Y.; Zhou, H. D.; Schlottmann, P. *Phys. Rev. Lett.* **2012**, *109*, 257205.

(15) Kenzelmann, M.; Lawes, G.; Harris, A. B.; Gasparovic, G.; Broholm, C.; Ramirez, A. P.; Jorge, G. A.; Jaime, M.; Park, S.; Huang, Q.; Shapiro, A. Ya.; Demianets, L. A. *Phys. Rev. Lett.* **2007**, *98*, 267205.
(16) White, J. S.; Niedermayer, Ch.; Gasparovic, G.; Broholm, C.; Park, J. M. S.; Shapiro, A. Ya.; Demianets, L. A.; Kenzelmann, M. *Phys. Rev. B* **2013**, *88*, 060409(R).
(17) Collins, M. F.; Petrenko, O. A. *Can. J. Phys.* **1997**, *75*, 605−655.
(18) Serrano-González, H.; Bramwell, S. T.; Harris, K. D. M.; Kariuki, B. M.; Nixon, L.; Parkin, I. P.; Ritter, C. *Phys. Rev. B* **1999**, *59*, 14451.
(19) Greedan, J. E. *J. Mater. Chem.* **2001**, *11*, 37−53.
(20) Svistov, L. E.; Smirnov, A. I.; Prozorova, L. A.; Petrenko, O. A.; Demianets, L. N.; Shapiro, A. Ya. *Phys. Rev. B* **2003**, *67*, 094434.
(21) Svistov, L. E.; Smirnov, A. I.; Prozorova, L. A.; Petrenko, O. A.; Micheler, A.; Büttgen, N.; Shapiro, A. Ya.; Demianets, L. N. *Phys. Rev. B* **2006**, *74*, 024412.
(22) Smirnov, A. I.; Yashiro, H.; Kimura, S.; Hagiwara, M.; Narumi, Y.; Kindo, K.; Kikkawa, A.; Katsumata, K.; Shapiro, A. Ya.; Demianets, L. N. *Phys. Rev. B* **2007**, *75*, 134412.
(23) Inami, T. *J. Solid State Chem.* **2007**, *180*, 2075−2079.
(24) Smirnov, A. I.; Svistov, L. E.; Prozorova, L. A.; Zheludev, A.; Lumsden, M. D.; Ressouche, E.; Petrenko, O. A.; Nishikawa, K.; Kimura, S.; Hagiwara, M.; Kindo, K.; Shapiro, A. Ya.; Demianets, L. N. *Phys. Rev. Lett.* **2009**, *102*, 037202.
(25) Hearmon, A. J.; Fabrizi, F.; Chapon, L. C.; Johnson, R. D.; Prabhakaran, D.; Streltsov, S. V.; Brown, P. J.; Radaelli, P. G. *Phys. Rev. Lett.* **2012**, *108*, 237201.
(26) Rodriguez-Cavajal, J. *FullProf*, version 2.05; Laboratoire Léon Brillouin CEA-CNRS: Gif-sur-Yvette, Cedex, France, 2011.
(27) Möller, A.; Amuneke, N. E.; Daniel, P.; Lorenz, B.; de la Cruz, C. R.; Gooch, M.; Chu, P. C. W. *Phys. Rev. B* **2012**, *85*, 214422.
(28) Bratsch, M.; Tapp, J.; Litvinchuk, A. P.; Möller, A. *Inorg. Chem.* **2014**, *53*, 4994−5001.
(29) Moessner, R.; Ramirez, A. R. *Phys. Today* **2006**, *59*, 24−29.
(30) Ramirez, A. P. *Annu. Rev. Mater. Sci.* **1994**, *24*, 453−80.
(31) Gągor, A.; Zajdel, P.; Többens, D. *J. Alloys Compd.* **2014**, *607*, 104−109.
(32) Becht, G. A.; Vaughey, J. T.; Hwu, S.-J. *Chem. Mater.* **2010**, *22*, 1149−1154.
(33) Du, A.; Wei, G. Z.; Li, J. *Phys. Stat. Sol. B* **2002**, *234*, 636−643.
(34) Fishman, R. S. *Phys. Rev. Lett.* **2011**, *106*, 037206.
(35) Terada, N.; Khalyavin, D. D.; Manuel, P.; Tsujimoto, Y.; Knight, K.; Radaelli, P. G.; Suzuki, H. S.; Kitazawa, H. *Phys. Rev. Lett.* **2012**, *109*, 097203.
(36) Terada, N.; Khalyavin, D. D.; Manuel, P.; Osakabe, T.; Radaelli, P. G.; Kitazawa, H. *Phys. Rev. B* **2014**, *89*, 220403(R).